

Effect of Hydrogen on Cavitation Erosion Behaviour of High Strength Steel

Y. X. Qiao^{1,*}, X. Cai¹, C. Ouyang^{1,*}, Y. G. Zheng²

¹ Jiangsu University of Science and Technology, 212003, Jiangsu, P. R. China

² Institute of Metal Research, Chinese Academy of Sciences, Shenyang 110016, Liaoning, P.R.China

*E-mail: yxqiao@imr.ac.cn, oyc1014@163.com

Received: 6 July 2016 / Accepted: 30 September 2016 / Published: 10 November 2016

The cavitation erosion behaviors of high strength steel electrochemically charged with hydrogen in distilled water and 3.5% NaCl solution were investigated. The results showed the surface hardness of the steel increased by electrochemical hydrogen-charging but no noticeable effect on the E_{corr} under condition of quiescence and cavitation respectively. Under condition of cavitation the corrosion rate was enhanced, especially for specimen electrochemically charged with hydrogen at $50 \text{ mA}\cdot\text{cm}^{-2}$ for 12 hours. The mass loss increased with the increasing of current density of electrochemical hydrogen-charging. The corrosion induced by erosion played an important role in the synergistic effect under condition of cavitation and electrochemistry was confirmed that hydrogen embrittlement had a great influence on cavitation erosion of high strength steel.

Keywords: A. Low alloy steel, B. Erosion, C. Hydrogen embrittlement, D. Hardening

1. INTRODUCTION

Cavitation characterized by vapor generation and condensation due to pressure changes. Pressure recovery causes these bubbles to implode in a few microseconds. These implosions or collapse generate pressure shockwaves, micro-liquid at a given temperature. Cavitation erosion occurs frequently in hydraulic machines resulting in mechanical degradation of metal materials. The embrittlement rupture of alloys resulting from aggressive medium has attracted more attentions of engineers and scientists in materials science and technology. OCV of corrosion, Mass loss, potentiodynamic polarization, electrochemical impedance spectroscopy (EIS), and scanning electron microscope are used to characterize properties of corrosion with and without cavitation in the medium.

Various stainless steels are used to investigate the mechanism of interaction of cavitation erosion and corrosion in distill water and sodium chloride solution[1]. With the growing application of

other metal materials (Ti alloy[2, 3], copper alloy[4], nickel-base alloy[5], Al alloys[6], etc.), their mechanism suffered from cavitation erosion are intensively researched. At the same time, surface modification of stainless steels(for example, laser surface alloying, Coating[7], etc.) applied in the surrounding of erosion are discussed. As shown above, not only phase of austenite, pearlite and ferrite, but also other phase and component are chosen to research the mechanism of cavitation erosion.

During the manufacture and service of steel components, hydrogen atoms are susceptible to permeate into the steel interior[8]. The potential process that can lead to this include cathodic protection, phosphating, pickling, electroplating and arc welding. In the different phases of steel, the contents of hydrogen are different. Zhu et al.[9] found that the hydrogen content in the retained austenite is three times greater than in martensite in this Q&P treated steel. Hydrogen-induced cracking can accelerate blocks of materials to split away off bulk. Hydrogen embrittlement should be a big problem of alloys under mechanical and chemical attacks simultaneously. The deleterious effect of hydrogen on mechanical properties was first documented by Johnson[10]. Hydrogen atoms, as a product of electrochemical processes such as cathodic reaction of corrosion, cathodic protection and electroplating, etc., may be adsorbed on the metal surface, diffused into metals and then influence the mechanical properties and electrochemical behavior of the metals[11-15]. High strength steels are known to exhibit a high susceptibility to hydrogen embrittlement compared with conventional construction steels [16-18]. Hydrogen embrittlement and its related mechanisms in steels had been studied extensively during the last several decades. Entry of hydrogen into materials is of serious concern to metallurgists and engineers, since it cause severely degeneration of the mechanical properties of metal. It can be generated simultaneously between erosion and corrosion, including cavitation and liquid erosion. The metal alloys loss rate can increase not only by the erosion and corrosion, but also their interaction of erosion and corrosion, which is called synergism. With another factor of hydrogen embrittlement, the synergism of erosion and corrosion will be affected a lot. However, most of previous studies were carried out on stress corrosion cracking, corrosion fatigue and the effect of hydrogen on mechanical properties of materials.

Up to now, the effect of hydrogen embrittlement on cavitation erosion resistance of alloys is rarely investigated [19-22]. Different currents are applied on the new high strength steels in order to charge hydrogen artificially. H is diffused into dislocation, boundary of grain and other places. Through electrochemical tests and topography after cavitation erosion, hydrogen embrittlement plays an important role in the process of corrosion and erosion. In our paper, we elaborate the mechanism of corrosion and erosion of high strength steel in two kinds of solution under effect of hydrogen embrittlement.

2. MATERIAL AND MEDIA

The chemical composition (wt.%) of high strength steel was 0.22% C, 1.10% Mn, 0.64% Si, 0.0021% P, 0.013% S and Fe balance. Its microstructure consisted of temper martensite on the surface. All of the specimen surfaces were prepared by final grinding with 800-grit abrasive paper. Then, the specimen were degreased by immersion in acetone (CH_3COCH_3) in an ultrasonic bath, rinsed with distilled water, then dried and stored in a desiccator. Before CE test, specimens were electrolytically

charged with hydrogen at room temperature in solution of 0.5 mol/L H₂SO₄. The current densities of 10, 20, 50 mA·cm⁻² were applied between the specimen and a platinum anode for 12 hours.

Cavitation was produced by a magnetostrictive-driven apparatus as introduced in previous literature[23], resonating at 20kHz with peak-to-peak amplitude of 60μm. This test followed ASTM Standard G32-92. A stainless steel beaker was surrounded by cooling water, in which 1250 mL of test medium was contained, and its temperature was maintained at room temperature (20±1°C). The solutions were exposed to air during the experiments. The cavitation tests were performed in distilled water (DW) and 3.5% NaCl (SW) solutions.

For cavitation erosion test, the specimen was immersed into the test medium to a depth of 15 mm. After each test period, the specimen was degreased, rinsed, dried, and weighed using an analytical balance with an accuracy of 0.1 mg. The erosion damage of the steel was expressed in term of mass loss and mass loss rate.

The electrochemical data were measured in-situ using a three-electrode electrochemical cell composed of a saturated calomel reference electrode (SCE) and a platinum flake as the counter electrode by IM6E electrochemical work station. Potentiodynamic polarization was swept from -500 mV to +800 mV relative to corrosion potential at a fixed rate of 0.5 mV/s. Linear polarization resistance (R_p) was measured by polarizing the specimen ±10mv relative to corrosion potential with a sweep rate of 0.166 mV/s. Electrochemical impedance spectra (EIS) measurement was conducted using a sinusoidal potential perturbation of 20mv in a frequency range from 10 mHz to 10 kHz.

Scanning electron micrographs (SEM) examination was performed on the specimen surface after cavitation for different periods to observe the developments of damage and on the cross-sections to observe the crack profile. The cross-sectional specimens were polished down to 1.5μm alumina powder, then etched using a 5% nital solution. The microhardness of the tested steel with or without electrochemical hydrogen-charging for 12h at various current density was determined with a microhardness tester using an applied load of 10 g (Laihua HVS-1000, China). To ensure reproducibility of the results, every test was repeated at least two times.

3. RESULTS

3.1 Surface hardness change caused by electrochemical hydrogen-charging

The surface hardness caused by electrochemical hydrogen-charging is shown in Fig. 1. The ingress of the hydrogen can result in the increase of the surface hardness. The value of current density has no obvious effect on surface hardness change of specimens. The fact that the amount of hydrogen-induced hardening is almost independent of the hydrogen concentration (the charging current density) is in agreement of the results reported by K. Oguri et.al[24]. The hardness of hydrogen reduced specimens is 1.1 times compared with that of unintroduced specimen. Essentially, three steps were involved during cathodic H⁺ reduction process. They are: (1) the hydrogen discharge reaction (proton tunneling), (2) hydrogen recombination reaction either by chemical recombination or electrochemical desorption, and (3) hydrogen permeation (mainly by bulk diffusion). After cathodic charging,

hydrogen after diffusion into the interior of matrix could be trapped at sites such as dislocations, grain boundaries, interfaces between different phases, or voids or cracks[25]. This implied that dislocation motion or dislocation source was inhibited to some extent by hydrogen in some extent during deformation. Therefore, micro-hardness of high strength steels are higher than that of without H⁺ reduction because dislocation motion is affected by hydrogen.

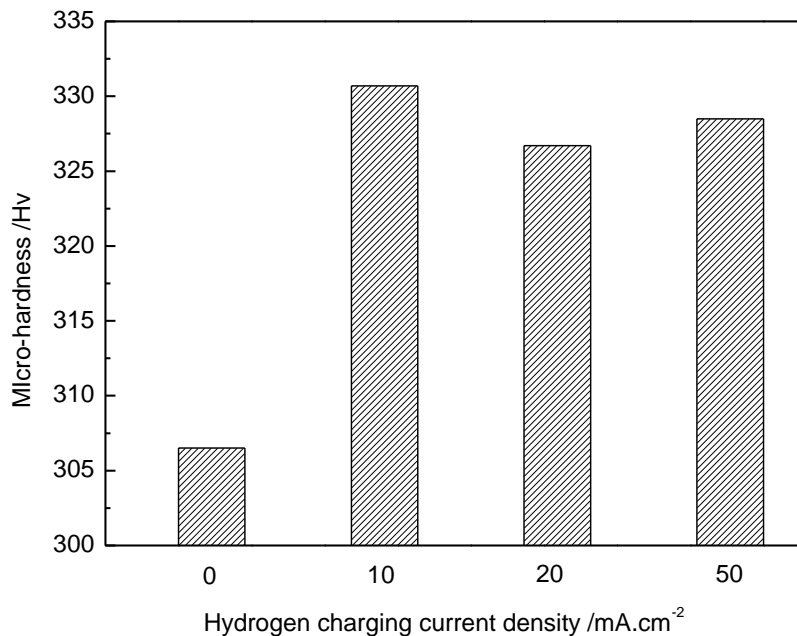
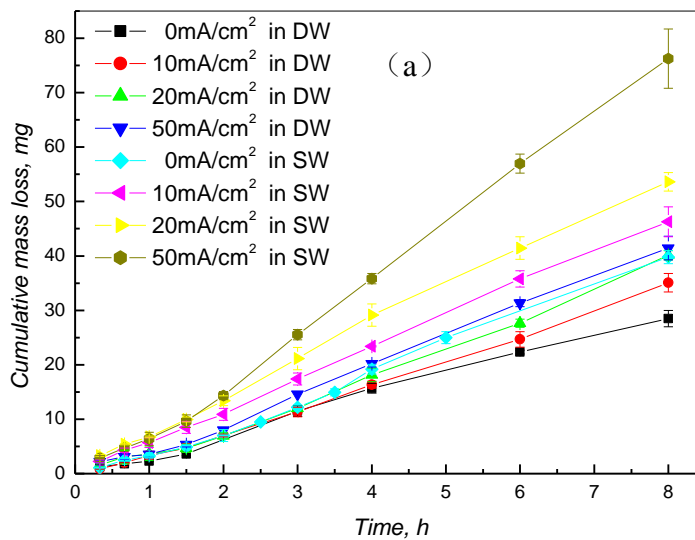


Figure 1. Micro-hardness of tested steel after electrochemical hydrogen-charging for 12h at various current density

3.2. Cumulative mass loss of tested steel in distilled water and 3.5% NaCl



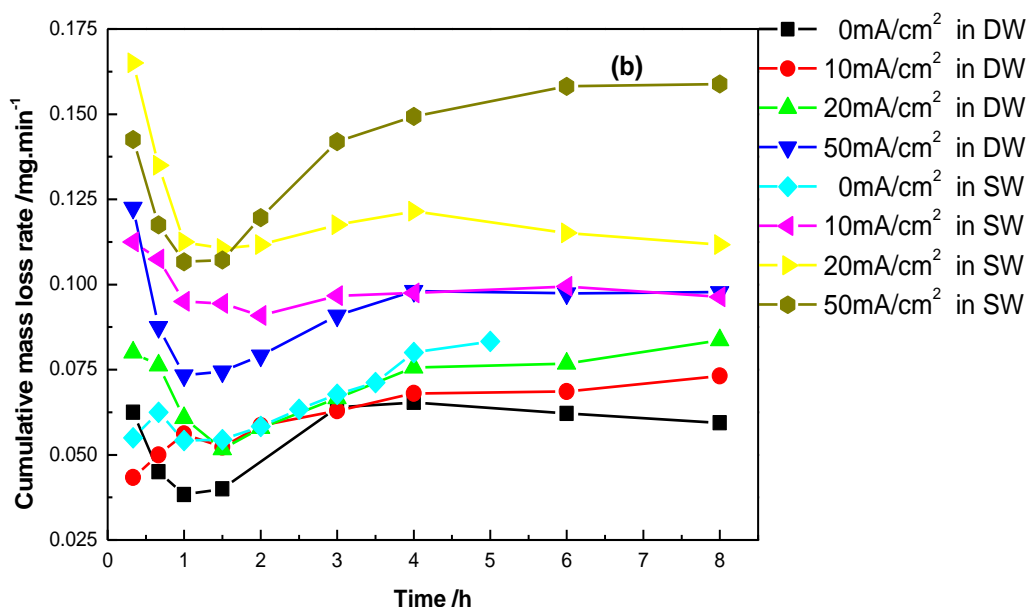


Figure 2. Cumulative mass loss (a) and mass loss rate (b) as a function of time for tested steel in distilled water and 3.5%NaCl

Table 1. Weight loss in cavitation erosion test after 8 h

Sample	Specimen in distilled water		Specimen in 3.5% NaCl	
	Mass loss (g)	Mass loss ratio	Mass loss (g)	Mass loss ratio
Uncharged	28.50	1.00	39.80	1.00
10 mA·cm ⁻²	35.10	1.23	46.25	1.16
20 mA·cm ⁻²	38.15	1.34	55.50	1.39
50 mA·cm ⁻²	41.45	1.46	76.25	1.92

The cumulative weight loss and mass loss rate as a function of the cavitation erosion test time in distilled water and 3.5% NaCl solution were shown in Fig. 2. Fig.2 (a) presents the cumulative mass loss as a function of the cavitation erosion test time in distilled water and 3.5% NaCl solution. The cavitation erosion resistance of uncharged specimen was higher than that of electrochemically hydrogen charging specimens. At the same charge current density the mass loss in 3.5% NaCl solution was higher than that in distilled water. The change in cavitation erosion resistance, as reflected by the mass loss in electrochemical hydrogen-charging and uncharged specimen, was given in Table 1. It could be observed that the resistance was significantly reduced by hydrogen pre-charging in all cases. It was confirmed that hydrogen embrittlement played an important role in mass loss of tested steel. Fig. 2(b) shows the relationship between cumulative mass loss rate and the cavitation erosion test time in distilled water and 3.5% NaCl solution. The mass loss rate rapidly decreased to a minimum after 1h, then increased slightly during cavitation to a maximum at 4h and then maintained a stable value up to 8h.

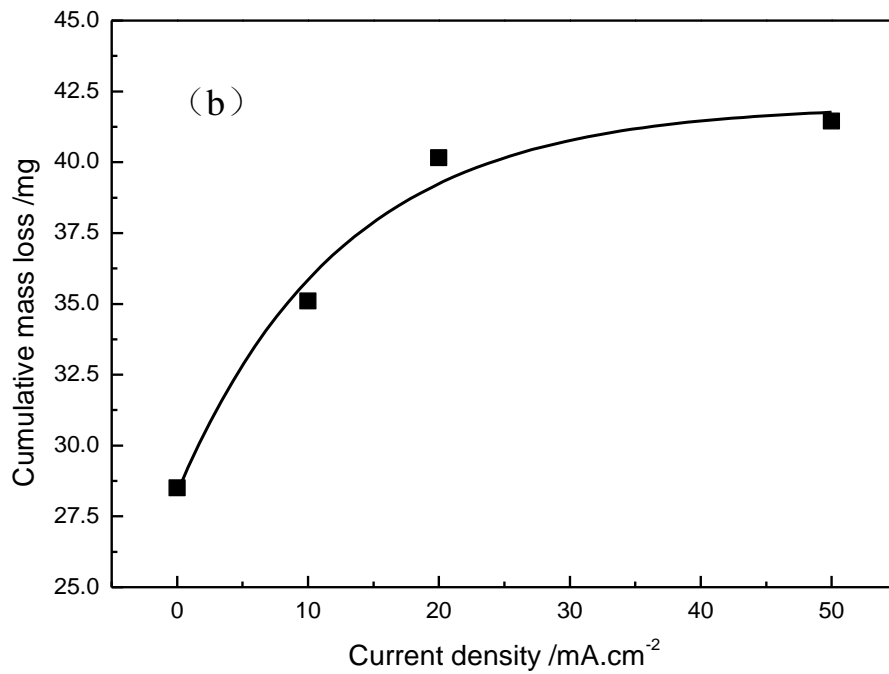
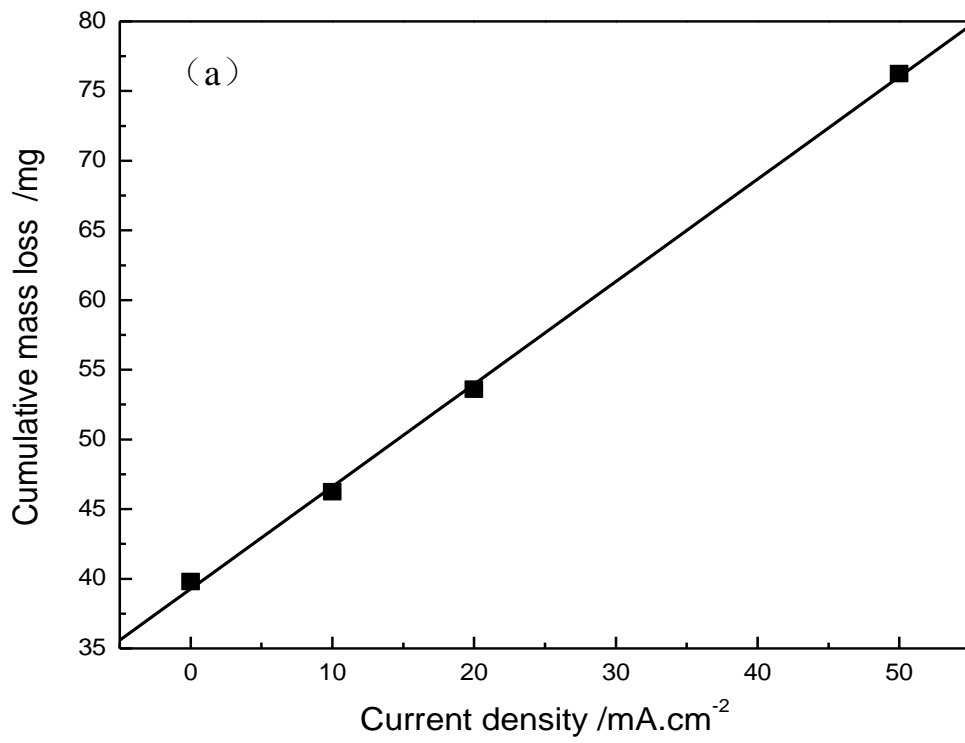


Figure 3. Cumulative mass loss for tested steel after cavitation erosion for 8h as a function of current density under cavitation condition in (a) distilled water and (b) 3.5% NaCl

Fig. 3 shown the mass loss of tested steel vs. current density after cavitation for 8 h in distilled water and 3.5% NaCl solution. Mass loss in 3.5% NaCl solution was linear with the increase of current density.

3.3 Electrochemical behavior

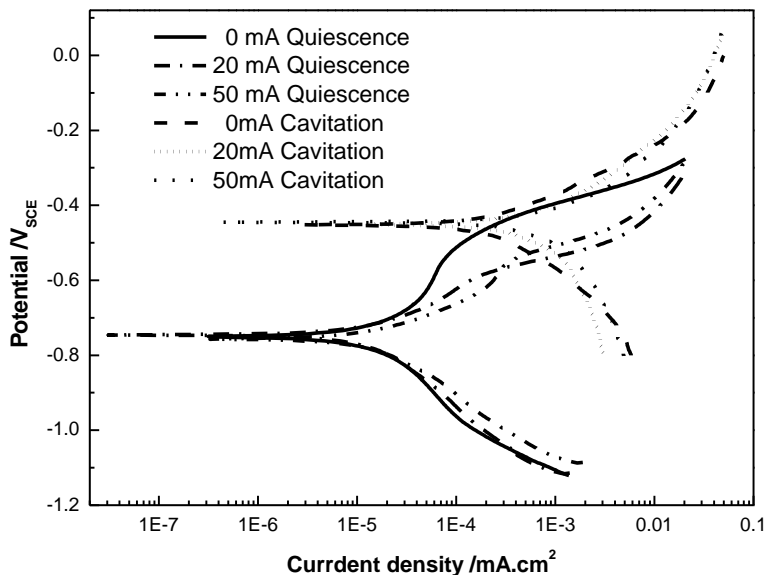
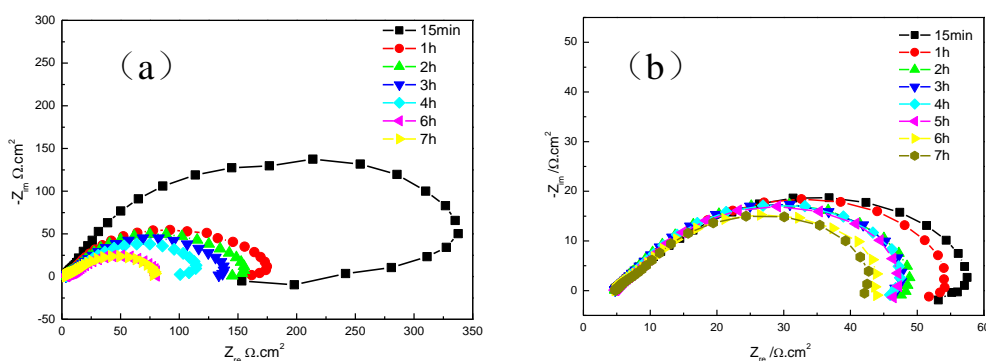


Figure 4. Potentiodynamic polarization curves for tested steel in 3.5% NaCl solution under static and cavitation condition

Table 2. Corrosion potential and corrosion current density of tested steel at 3.5 % NaCl

Hydrogen charging current density (mA·cm ⁻²)	Quiescence		Cavitation	
	<i>E_{corr}</i> (V _{SCE})	<i>i_{corr}</i> × 10 ⁻⁵ (A·cm ⁻²)	<i>E_{corr}</i> (V _{SCE})	<i>i_{corr}</i> × 10 ⁻⁵ (A·cm ⁻²)
0	-0.75	1.67	-0.45	0.19
20	-0.75	1.79	-0.45	0.34
50	-0.76	1.82	-0.44	0.48



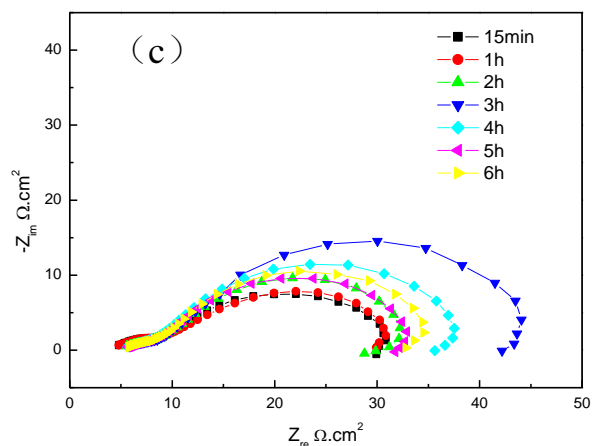
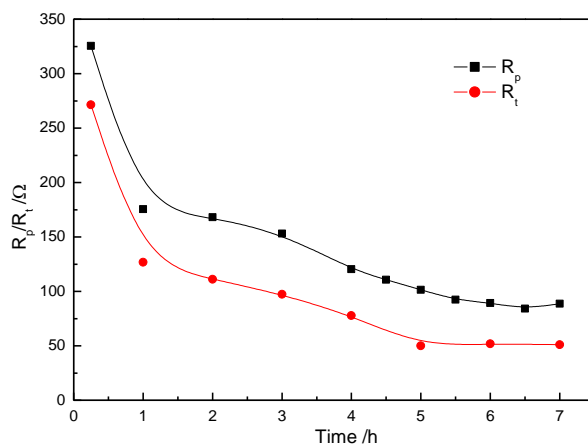


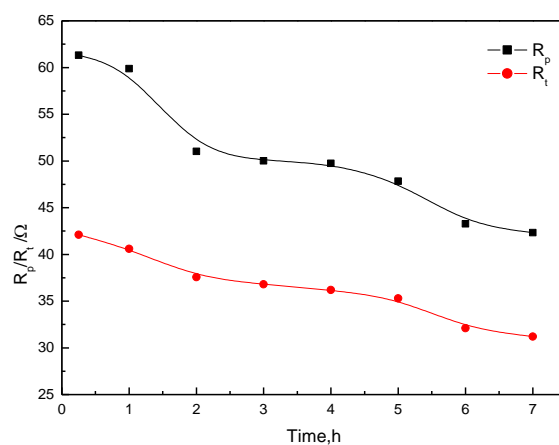
Figure 5. Nyquist plots measured at various time for tested steel in 3.5%NaCl solution under cavitation condition (a)uncharged (b)20mA·cm⁻²(c)50mA·cm⁻²

Figure 4 shown the potentiodynamic polarization curves of specimen under quiescent and CE condition. The current density (i_{corr}) value obtained by the Tafel extrapolation and free corrosion potential (E_{corr}) were listed in Table 2. Electrochemical hydrogen-charging had no obvious effect on the E_{corr} of tested steel under quiescent and cavitation condition. But electrochemical hydrogen charging can remarkably increase the anodic dissolution of steel under quiescent condition. The cathodic current density of electrochemical hydrogen-charging sample was only slightly bigger than that of un-charged sample. The anodic dissolution rate of electrochemical hydrogen-charging specimen was 10 times than that of un-charged specimen at same corrosion potential. The Cavitation strongly affected the polarization behavior of tested steel. Cavitation shifted the corrosion potential to the positive direction from -750 mV vs. SCE to -450 mV vs. SCE. The polarization current density under cavitation condition was larger than that of under quiescent condition. The cathodic reaction dramatically enhanced by cavitation while the effect of cavitation on anodic reaction was not very obvious. That was to say that the corrosion rate increased a lot by cavitation and corrosion played an important role under cavitation condition.

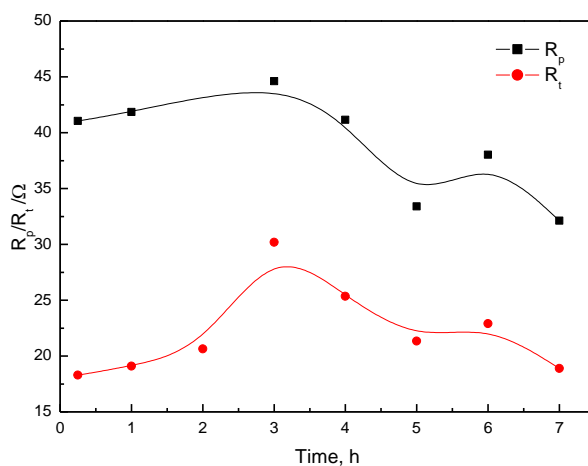
The impedance spectra measured in the presence of cavitation with or without electrochemical hydrogen-charging were presented in Nyquist plots in Fig. 5. In all Figs, these plots showed that a well-defined semicircle was presented in the high frequency range in the absence of cavitation with or without electrochemical hydrogen-charging, while an inductive segment was presented in the low-frequency range. From Fig. 5(a) and (b) the magnitude of impedance rapidly decreased within 5h and then leveled off with a slow decrease after 5h of cavitation. In Fig. 5(c) the magnitude of impedance increased to a maximum at 3h then decreased. It is reported that during electrochemical hydrogen-charging hydride and tiny cracks may produce on the sample surface[26]. This phenomenon may relate to the deterioration of material properties due to H⁺ reduction and CE damage.



(a)



(b)

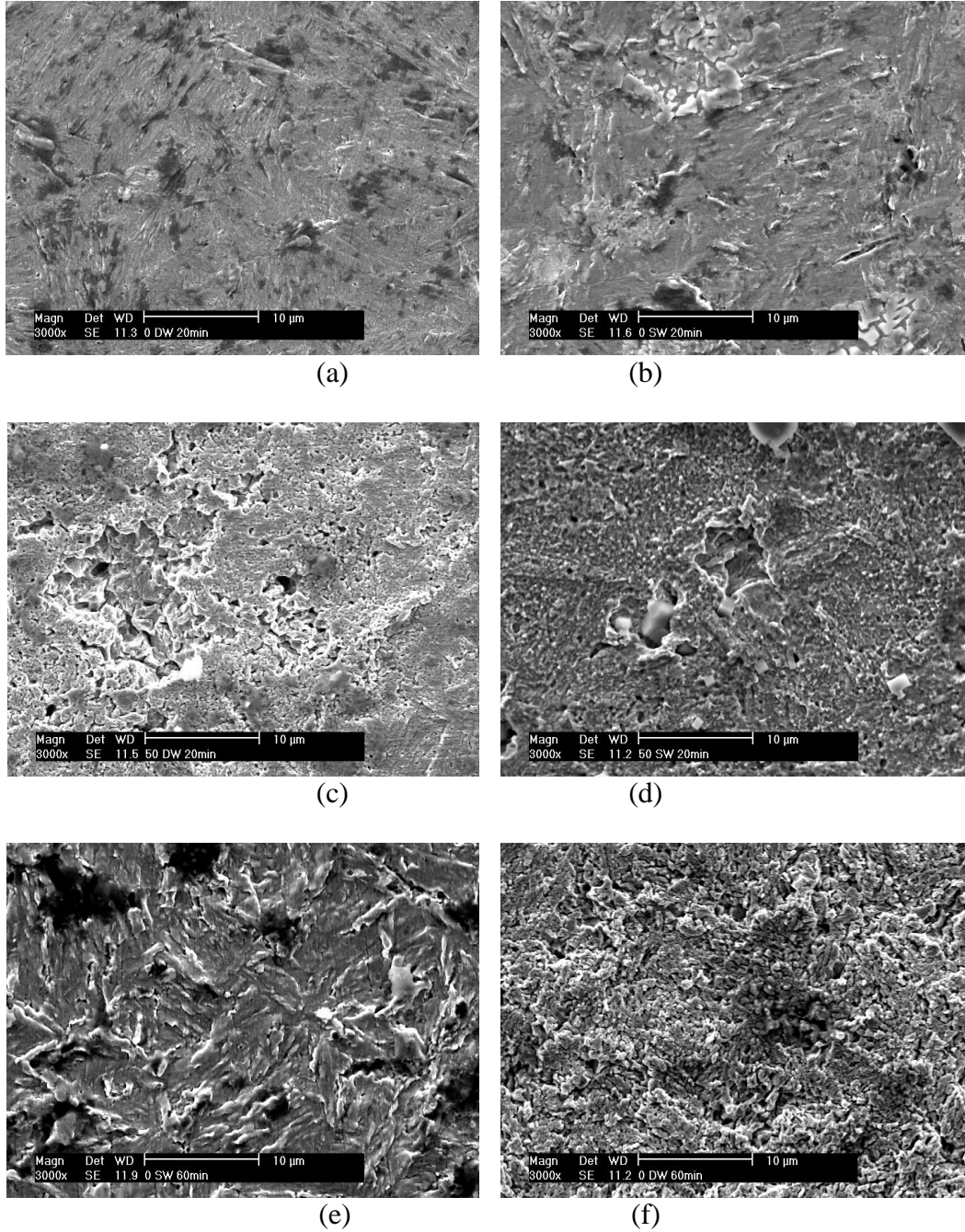


(c)

Figure 6. R_p and R_t at various time for tested steel in 3.5%NaCl solution under cavitation condition (a)uncharged (b)20mA·cm⁻²(c)50mA·cm⁻²

Fig.6 shown that both linear polarization resistance (R_p) and charge-transfer resistance (R_{ct}), which was obtained from the analysis of impedance spectra in Fig. 6, had the same trend during the experiment.

3.4 Morphologies of eroded surfaces and cross-sectional crack propagation of tested steel



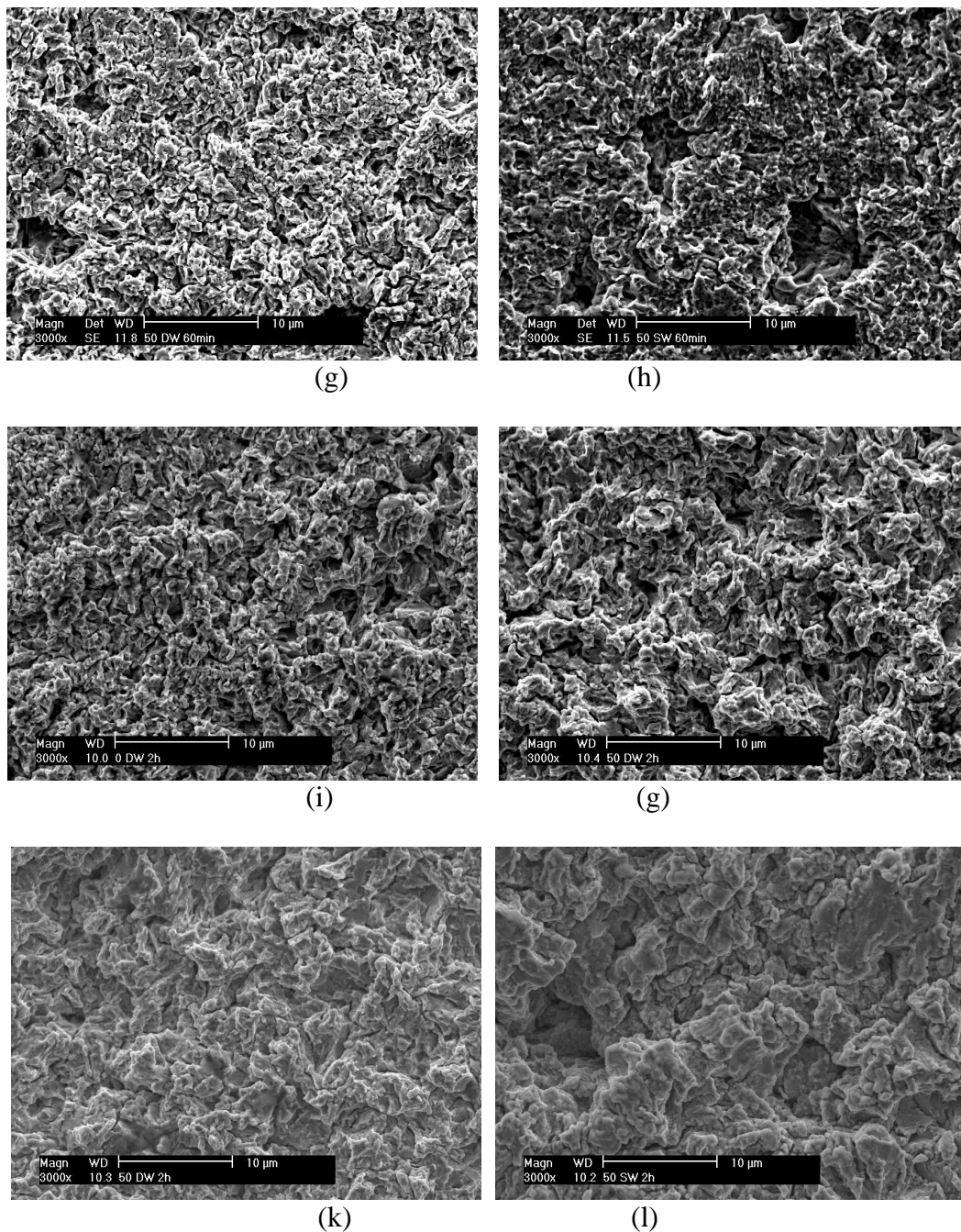


Figure 7. Morphologies of tested steel after cavitation erosion for different duration

- (a) (e) (i) uncharged specimen in distilled water
- (b) (f) (g) uncharged specimen in 3.5% NaCl
- (c) (j) (k) $50\text{mA}\cdot\text{cm}^{-2}$ charge in distilled water
- (d) (h) (l) $50\text{mA}\cdot\text{cm}^{-2}$ charge in 3.5% NaCl
- (a)—(d) 20min (e) —(h) 60min (i) —(l) 120min

Fig. 7 showed SEM of eroded surfaces of the tested steel subjected to various periods of CE testing. After CE for 20 min, no any obvious mass loss can be seen on the surface of uncharged specimen, as was shown in Fig. 7a and Fig. 7b. As for electrochemical hydrogen-charging specimen,

only cavitation pit could be seen on the surface of specimen tested in distilled water, while the whole surface has been completely removed by cavitation attack in 3.5% NaCl solution as shown in Fig. 7c and Fig. 7d. With the increasing of CE periods (60 min), the deformation of martensite lathings was mainly restrained by their boundaries, as shown in Fig. 7e. In Fig. 7f, Fig. 7g and Fig. 7h, the whole surface is completely damaged and several pits could be seen in Fig. 8h. With longer CE duration (120min), as shown in fig.7i, 7g, 7k, 7l, the specimens had been seriously damaged and the layer of tempered martensite had been completely removed. The cavitation erosion resistance of tested steel with and without electrochemical hydrogen-charging in distilled water was higher than of in 3.5% NaCl solution. The cavitation erosion resistance of tested steel without hydrogen charging was higher than that of electrochemical hydrogen-charging in same solution.

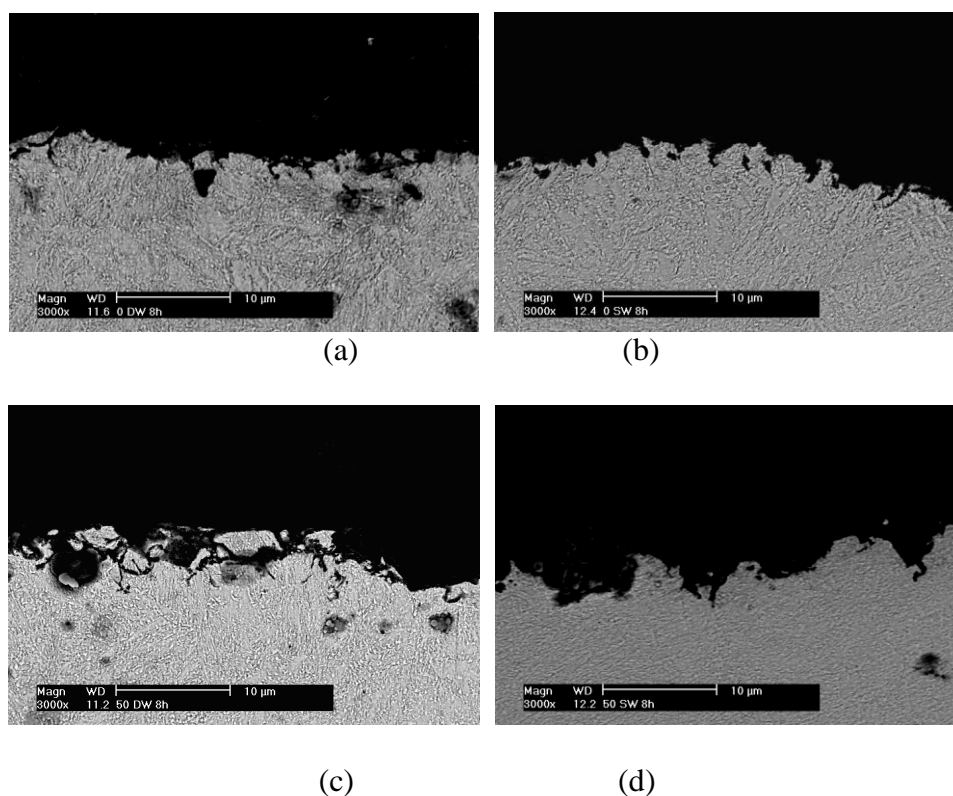


Figure 8. Morphologies for cross-section of tested steel after cavitation erosion for 8h
 (a) uncharged specimen in distilled water (b) uncharged specimen in 3.5% NaCl
 (c) 50 mA·cm⁻² charge in distilled water (d) 50 mA·cm⁻² charge in 3.5% NaCl

Fig. 8 showed SEM morphologies of cross-sectional cracks of tested steel with and without electrochemical hydrogen-charging after cavitation erosion for 8h in distilled water and 3.5%NaCl solution. The cracks in tested steel were nearly parallel to each other and perpendicular to the eroded surface. The cracks of specimen in 3.5% NaCl solution were deeper and wider than that of in distilled water. The cracks of specimen with electrochemical hydrogen-charging were wider, deeper and more rounded than that of in un-charged specimen.

4. DISCUSSION

4.1 Role of hydrogen on cavitation erosion crack propagation of high strength steel

Localization of hydrogen atoms could occur at trapped sites such as dislocations, grain boundaries, interfaces between different phases, or voids or cracks within which hydrogen atoms could be surface adsorbed and recombined. Localization of hydrogen atoms could also occur through the effect of stress on the chemical potential of hydrogen atoms[27]. Regions of hydrostatic stress were regions of low chemical potential and hydrogen atoms will diffuse spontaneously to this region, thereby which raising the local concentration of hydrogen atoms. Diffusion of hydrogen atoms according to the following equation:

$$\mu - \mu_0 = \int_V \sigma_{ij} \varepsilon_{ij} dV \quad (2)$$

Here μ and μ_0 represented the chemical potential with and without hydrostatic stress, σ_{ij} represented applied stress, ε_{ij} represent the strain energy around hydrogen atom. At steady-state the local chemical potential would be that of hydrogen atoms in the bulk material since the system would come to equilibrium. However concentration of local hydrogen atom would be elevated in relation to the surrounding unstressed matrix. The transport and localization of hydrogen atoms would be proceeding until the equilibrium state achieved. Under equilibrium state, the hydrogen concentration can be depicted by:

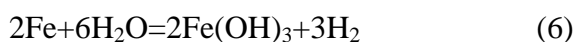
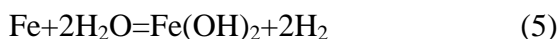
$$C = C_0 \exp \frac{\int_V \sigma_{ij} \varepsilon_{ij} dV}{Rt} \quad (3)$$

Here C_0 was the hydrogen concentration at stress free state ($\sigma_{ij}=0$). Assuming the stress was constant then the equation could be rewritten as:

$$C = C_0 \exp \frac{W \sigma_h \bar{V}_H}{Rt} \quad (4)$$

That was to say, hydrogen could spontaneously diffuse and concentrate in the crack tips because of the high stress concentration at these regions. Wang *et al.*[28] had observed the presence of hydrogen peak at the crack tip.

There were two kinds of hydrogen in tested steel which could concentration at crack tips. One came from the cathodic hydrogen charging process. The other came from the corrosion process of the tested steel and tested solution. Hydrogen easily penetrated into the high strength steel. As the increase of amount of hydrogen, the fracture surface ratio for steel increase[29]. As CE proceeded under the repeated stress induced by CE attack, the cracks formed and propagated in fatigue like manner and resulted in the materials loss. Once cracks forming, those cracks were immediately filled with tested solution. Oxygen in the bulk solution was difficult to attain cracks tips by diffusion. So, reduction of water became the dominant cathodic reaction at crack tips. In aqueous solutions hydrogen atoms were generated electrochemically on the metal surface as a partial cathodic reaction in the corrosion process. The basic reactions were represented by:

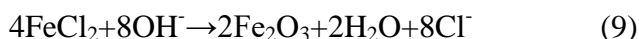


It was reported there was existence of a plastic zone at the front of the crack tip [30]. The existence of hydrogen atoms in crack tip material either in the plastic zone or in elastic zone could change its mechanical properties[31], which would change the size of plastic zone. Stress intensity factor K was proportion to the radius of plastic zone $r_0^{1/2}$. The dislocations surrounded by hydrogen atoms could also exert a sufficient stress intensity factor[21] at crack tips to cause propagation of cracks even without any externally applied stress.

The hydrogen atoms in material not only changed its mechanical properties but also lowered the local maximum cohesive force acting against the collinear separation of the metal atoms. That adsorption-induced weakening of interatomic bonds at crack tips reduce not only the stress required for tensile separation of atoms but also the stress necessary for shear movement of atoms at crack tips[32, 33]. Because of cavitation, cracks can be connected to drop as massive chunks, which is accelerated by hydrogen embrittlement[34]. Thus, it was envisaged that atomically brittle fracture could occur in normally ductile material because adsorption lowered the stress requiring for decohesion to a level below that required for slip at crack tips. Decohesion should produce atomically sharp crack tips. This was coincidence with the results presented in Fig. 8, that the crack in electrochemical hydrogen-charging sample was board and sharp compared with the tiny and short in uncharged sample.

4.2 Corrosion mechanisms of tested steel in NaCl solution

Oxygen depolarization corrosion occurred in most neutral media. Among process of corrosion, surface of steel can generate bubbles by the press and following collapse especially caused by flowing of fluid. As shown in figure2b, cumulative loss sharply decrease within one hour. The equation of reaction is shown above (Eq.5&6). The formation of precipitation on the surface of high strength steel delay the redox reaction. Cumulative loss rate of specimens increase around 1.5 hour after immersion. That is because Cl^- dissolves the precipitation. As shown equations below (Eq.7-9), FeCl_2 is formed. Fe_2O_3 as solid drop into the bottom of vessel[35, 36]. In neutral NaCl solution, the oxygen reduction was the predominant cathodic reaction and iron oxidation was the main anodic reaction. Previous studies showed that the presence of Cl^- ion accelerated corrosion. They participate in the following cycling process as a catalyzer although they could not form stable corrosion products in the solution. The mechanism of dissolution of iron in was as followed [37, 38]:



The main reaction was the oxidation to OH^- . In the solution Cl^- acted as a catalyzer. The corrosion product on sample surface was loose and lack of protective ability and easily reduced/removed under cavitation condition.

The impedance spectra measured in the presence of cavitation with or without electrochemical hydrogen-charging were presented in Nyquist plots in Fig. 5. In all Figs, these plots showed that a well-defined semicircle was presented in the high frequency range in the absence of cavitation with or without electrochemical hydrogen-charging, while an inductive segment was presented in the low-frequency range. From Fig. 5(a) and (b) the magnitude of impedance rapidly decreased within 5h and

then leveled off with a slow decrease after 5h of cavitation. In Fig. 5(c) the magnitude of impedance increased to a maximum at 3h then decreased. It is reported that during electrochemical hydrogen-charging hydride and tiny cracks may produce on the sample surface[26]. This phenomenon may relate to the deterioration of material properties due to H^+ reduction and CE damage.

4.3 Effect of cavitation on electrochemical behavior

According to the assumption, the cathodic reaction was mixed with charge transfer–mass transfer control and speed of flow of fluids. This reaction (reduction of O_2 to OH^-), therefore, was clearly influenced by mass transfer phenomena which was dependent on fluid dynamic conditions at the electrode surface. i_l was theoretically expressed by Levich's equation[39]:

$$i_l = 0.62nFD^{2/3}\nu^{-1/6}\omega^{1/2}C_0 \quad (10)$$

where i_l was the limiting cathodic current density; n was the number of transferred electrons involved in O_2 reduction; F was the Faraday constant; C_0 was the concentration of dissolved O_2 ; D was the diffusion coefficient of dissolved O_2 ; ν was the kinematic viscosity of the test solution and ω was the angular frequency of rotation. Based on the potentiodynamic polarization curves in Fig. 4, the trend observed in the cathodic current curves showed that cavitation erosion had a clear influence on the kinetics of oxygen reduction on tested steel. From the condition of quiescence and cavitation, the slope of cathodic lines were very different from each other. The cavitation on the fluid dynamic conditions of solution near electrode surface was similarly to the effect of rotate. Both of them increased the process of mass transfer in tested solution. According to Eq.10, the cathodic current increased with the increase of rotation rate.

The increase in the cathodic currents under cavitation condition was due to increase in the limiting current, i_l . The effect of cavitation on anodic polarization curves was little effect as shown in fig.4. This behaviour confirmed that the anodic parameters β_a and i_{0Fe} in fact independent of mass transfer influence and truly represent the intrinsic kinetic parameters associated to a pure charge transfer control [40]. In the process of cavitation, vibration and bubble can accelerate the flowing of redox specimens. Bubble breakup caused the instantaneous high press, which of effect was more obvious. Especially mass transfer of O_2 was improved one of magnitude as shown in current of Table 2. At the same time, precipitation and corrosion products on the surface of matrix were removed by flow of liquid. Accordingly charge transfer resistance decrease because of bare matrix and active surface was exposed to corrosive medium[41, 42].

4.4 The synergistic effect under cavitation condition

Many studies on cavitation erosion had been made and showed that both mechanical and electrochemical factors were involved. The conjoint action of electrochemical and mechanical factor would produce far more damage than if each acted separately in a large number of systems[20, 23, 43-45]. The total CE-corrosion mass loss was composed of an erosion mass loss, a corrosion mass loss and a synergistic effect between erosion and corrosion, which could be expressed by the following equation[23]:

$$W_T = W_E + W_C + W_{EIC} + W_{CIE} \quad (11)$$

where W_T was the total mass loss, W_E is the component of pure cavitation erosion which was supposed to be the mass loss in distilled water, W_C was the component of pure corrosion under quiescence condition, W_{EIC} and W_{CIE} were the component of erosion induced corrosion and the component of corrosion induced erosion, respectively.

Table 3. Contribution of mass loss in erosion (W_E), in corrosion (W_C), in erosion-induced corrosion (W_{EIC}) and in corrosion-induced erosion (W_{CIE}) for tested steel in 3.5 % NaCl after cavitation erosion for 8 h

Sample	Mass-loss rate (mg)				Damage fraction (%)				
	W_C	W_E	W_{EIC}	W_{CIE}	W_T	W_C	W_E	W_{EIC}	W_{CIE}
Uncharged	0.014	28.50	1.58	9.71	39.80	0.034	71.61	3.97	24.39
20 mA·cm ⁻²	0.015	38.15	2.29	15.05	55.50	0.027	69.36	4.13	27.90
50 mA·cm ⁻²	0.016	41.45	3.95	31.25	76.25	0.047	54.36	5.18	40.94

According to the value of i_{corr} in Table 2, the contribution of each part could be calculated by using Faraday's law. A corrosion current of 1mA was equal to a mass loss of 1.04 mg/h, assuming a density of 7.8×10^6 g/m³ and atom weight of iron of 55.85 for the tested steel. Thus, the W_C and W_{EIC} of tested steel in the test solution could be calculated, the same with the W_E and W_{CIE} . Table 3 presents the values of each component for both steels. It was clear that the amount of damage caused by pure corrosion is relatively small, and the synergistic of corrosion and erosion had a strong effect on the damage. This result suggested that W_{CIE} in the present work played an important role. W_E increase with the increase of current density, while W_{CIE} increased with the increase of current density. It was confirmed that the hydrogen embrittlement had a great influence on the cavitation erosion resistance of tested steel as shown in table.3, which surpassed the half percent of mass loss in the whole process of corrosion.

5. CONCLUSIONS

A preliminary study has been carried out to investigate the effect of electrolytic hydrogen pre-charging on the CE behavior of a high strength steel. The following conclusions are drawn as follows:

(1) Electrochemical charging hydrogen can increase the micro-hardness of tested steel and hydrogen-induced hardening is almost independent of the hydrogen concentration.

(2) Though hydrogen has no any obvious effect on the E_{corr} under quiescence and cavitation condition, but the corrosion resistance of tested steel can be reduced by electrochemical hydrogen charging.

(3) The mass loss increases with the increasing of current density. Under CE condition the corrosion rate is greatly enhanced, especially for specimen charged at $50\text{mA}\cdot\text{cm}^{-2}$. The corrosion induced erosion play an important role in the synergistic effect under cavitation condition.

(4) Hydrogen embrittlement has a great influence on cavitation erosion of high strength steel.

ACKNOWLEDGEMENTS

The authors would like to express their thanks to the Startup project of Doctor Scientific Research of Jiangsu University of Science and Technology for its financial support(No. 1062921401) and Professor Ziyong Zhu for providing the tested steel.

References

1. B. Vyas and I. L. H. Hansson, *Corrosion Science*, 30 (8–9) (1990) 761-770.
2. F. Dong, X. Li, L. Zhang, L. Ma and R. Li, *Ultrasonics Sonochemistry*, 31 (2016) 150-156.
3. I. Mitelea, E. Dimian, I. Bordeasu and C. Crciunescu, *Ultrasonics Sonochemistry*, 21 (4) (2014) 1544-1548.
4. J. Stella, M. Pohl, C. Bock and U. Kunze, *Wear*, 316 (1–2) (2014) 1-5.
5. M. C. Park, G. S. Shin, J. Y. Yun, J. H. Heo, D. I. Kim and S. J. Kim, *Wear*, 310 (1–2) (2014) 27-32.
6. F. Cheng, S. Jiang and J. Liang, *Applied Surface Science*, 280 (2013) 287-296.
7. J. Stella, E. Schller, C. Heing and O. A. Hamed, *Wear*, 260 (9-10) (2006) 1020-1027.
8. J. Yang, F. Huang, Z. Guo, Y. Rong and N. Chen, *Materials Science and Engineering: A*, 665 (2016) 76-85.
9. X. Zhu, W. Li, H. Zhao, L. Wang and X. Jin, *International Journal of Hydrogen Energy*, 39 (24) (2014) 13031-13040.
10. William H. Johnson, *Nature*, 11 (281) (1970) 393.
11. R. H. Song, S. I. Pyun and R. A. Oriani, *Journal of the Electrochemical Society*, 137 (6) (1990) 1703-1706.
12. H. R. Gray and Y. aoyama, *Corrosion -Houston Tx-*, 28 (2) (1972) 459-466.
13. L. J. Qiao, C. M. Hsiao, W. Y. Chu, L. Chen, S. W. Liu and J. J. Zou, *Advanced Materials Research*, 22 (5) (1988) 627-630.
14. G. Razzini, S. Maffi, G. Mussati and L. P. Bicelli, *Corrosion Science*, 37 (7) (1995) 1131-1141.
15. G. Razzini, S. Maffi, G. Mussati, L. P. Bicelli and G. Mitsi, *Corrosion Science*, 39 (4) (1997) 613-625.
16. K. Tsuboi, H. Yatabe and K. Yamada, *Materials Science & Technology*, 12 (5) (1996) 400-404.
17. I. O. Shim and J. G. Byrne, *Materials Science & Engineering A*, 123 (2) (1990) 169-180.
18. D. Hardie and S. E. Liu, *Corrosion Science*, 38 (5) (1996) 721-733.
19. K. Ogino, A. Hida and S. Kishima, *Corrosion -Houston Tx-*, 44 (2) (1988) 97-103.
20. C. T. Kwok, F. T. Cheng and H. C. Man, *Materials Science & Engineering A*, 290 (1-2) (2000) 145–154.
21. Y. G. Zheng, S. Z. Luo and W. Ke, *Tribology International*, 41 (12) (2008) 1181-1189.
22. Y. X. Qiao, Y. G. Zheng, X. Q. Wu, W. Ke, K. Yang and Z. H. Jiang, *Tribology - Materials Surfaces & Interfaces*, 1 (3) (2007) 165-172.
23. S. Z. Luo, M. C. Li, W. Z. Ke, Z. M. Yao and Y. G. Zheng, *Corrosion -Houston Tx-*, 59 (7) (2003) 597-605.
24. K. Oguri, S. Takaki and H. Kimura, *Materials Science & Engineering*, 53 (2) (1982) 223-232.
25. A. Zielinski, E. Lunarska, P. Michalak and W. Serbinski, *Materials Science*, 40 (6) (2004) 822-830.

26. F. T. Cheng, P. Shi and H. C. Man, *Scripta Materialia*, 47 (2) (2002) 89-94.
27. R. Liu, N. Narita, C. Altstetter, H. Birnbaum and E. N. Pugh, *Metallurgical & Materials Transactions A*, 11 (9) (1980) 1563-1574.
28. Z. F. Wang, J. Li, W. Ke and Z. Zhu, *Fatigue & Fracture of Engineering Materials & Structures*, 16 (16) (1993) 441-451.
29. K. Takasawa, Y. Wada, R. Ishigaki and R. Kayano, *Materials Transactions*, 74 (8) (2010) 520-526.
30. A. V. Babak and E. I. Uskov, *Strength of Materials*, 15 (5) (1983) 667-672.
31. J. P. Hirth and J. R. Rice, *Metallurgical Transactions A*, 11 (9) (1980) 1501-1511.
32. M. E. Eberhart, K. H. Johnson and R. M. Latanision, *Acta Metallurgica*, 32 (6) (1984) 955-959.
33. R. A. Oriani, *Scripta Metallurgica*, 18 (3) (1984) 265-268.
34. Y. G. Zheng, S. Z. Luo and W. Ke, *Tribology International*, 41 (12) (2008) 1181-1189.
35. C. Yk, C. Sl and B. Ce, *International Journal of Multiphase Flow*, 293 (-1) (1995) 99-126.
36. S. A. Karrab, M. A. Doheim, M. S. Mohammed and S. M. Ahmed, *Tribology Letters*, 45 (3) (2012) 437-444.
37. S. B. Lalvani and G. Zhang, *Corrosion Science*, 37 (10) (1995) 1567-1582.
38. S. Arzola, M. E. Palomar-Pardavé and J. Genesca, *Journal of Applied Electrochemistry*, 33 (12) (2003) 1233-1237.
39. D. B. Spalding, *International Journal of Heat & Mass Transfer*, 6 (10) (1963) 931-932.
40. L. Cáceres, T. Vargas and L. Herrera, *Corrosion Science*, 49 (8) (2007) 3168-3184.
41. M. R. Hoffmann, I. Hua and R. Höchemer, *Ultrasonics Sonochemistry*, 3 (3) (1996) S163-S172.
42. S. J. Lee, *Transactions of Nonferrous Metals Society of China*, 21 (8) (2011) 1703-1709.
43. C. T. Kwok, P. K. Wong, H. C. Man and F. T. Cheng, *International Journal of Railway*, 3 (2010) 19-27.
44. W. J. Tomlinson and M. G. Talks, *Journal of Materials Science*, 26 (3) (1991) 804-808.
45. A. Karimi and J. L. Martin, *International Materials Reviews*, 31 (2013) 219-224.